https://doi.org/10.5194/egusphere-2025-987
Preprint. Discussion started: 21 March 2025

Bottom–up approach for mitigating extreme events under limited intervention options: a case study with Lorenz 96

Takahito Mitsui[1], Shunji Kotsuki[2,3], Naoya Fujiwara[4], Astushi Okazaki[2,3], and Keita Tokuda[1]

[1]Faculty of Health Data Science, Juntendo Univerity, Urayasu, Japan
[2]Institute for Advanced Academic Research, Chiba University, Chiba, Japan
[3]Center for Environmental Remote Sensing, Chiba University, Chiba, Japan
[4]Graduate School of Information Sciences, Tohoku University, Sendai, Japan

Correspondence: Takahito Mitsui (takahito321@gmail.com)

Abstract. Prediction and mitigation of extreme weather events are important scientific and societal challenges. Recently, Miyoshi and Sun (2022) proposed a control simulation experiment framework that assesses the controllability of chaotic systems under observational uncertainty, and within this framework, Sun et al. (2023) developed a method to prevent extreme events in the Lorenz 96 model. However, since their method is primarily designed to apply control inputs to all grid variables, the success rate decreases to approximately 60% when applied to a single site, at least in a specific setting. Herein, we propose an approach that mitigates extreme events through local interventions based on multi-scenario ensemble forecasts. The success rate of our method is markedly higher than that of Sun et al.'s method, reaching 94% even when applying interventions at one site per step, albeit with a moderate increase in the intervention cost. Furthermore, the success rate increases to 99.4% during interventions at two sites. Unlike control-theoretic approaches adopting a top–down strategy, which determine inputs by optimizing cost functions, our bottom–up approach mitigates extreme events by effectively utilizing limited intervention options.

1 Introduction

Global warming has likely increased the frequency and intensity of extreme weather events worldwide, such as heatwaves and heavy rainfall (IPCC, 2023). These threats are expected to escalate during the present century. Efforts to mitigate the risks posed by extreme events include advancements in weather forecasting and the development of disaster-resilient infrastructures. More ambitious projects have focused on active manipulation of weather systems. A prominent example is Project STORMFURY conducted by the U.S. government from 1962 to 1983, which aimed to weaken tropical cyclones by seeding them with silver iodide, although the initially promising results of this study were questioned in later studies (Willoughby et al., 1985).

Artificial weather control faces several fundamental challenges. First, meso- or synoptic-scale weather systems, such as stationary rainbands and tropical cyclones, are significantly larger in scale than what we can feasibly influence through interventions. Second, weather systems are inherently chaotic and sensitive to the initial conditions, limiting system predictability. Observational uncertainties and discrepancies between models and reality further increase the complexity (Palmer and Hage-

https://doi.org/10.5194/egusphere-2025-987
Preprint. Discussion started: 21 March 2025

dorn, 2006). Consequently, predicting the outcomes of interventions is inherently difficult. This paper proposes a mathematical approach to alleviate these challenges.

Several mathematical algorithms have been proposed for mitigating extreme weather events through interventions. Henderson et al. (2005) proposed a method using the four-dimensional variational data assimilation to identify the smallest temperature increments required for minimizing wind damage during a hurricane. Miyoshi and Sun (2022) proposed a framework called the Control Simulation Experiment (CSE), which extends the concept of observing system simulation experiments to investigate the controllability of dynamical systems under observational uncertainty. Their CSE successfully prevents regime transitions in the Lorenz 63 model, whereas the CSE application of Sun et al. (2023) reduces the number of extreme events in the Lorenz 96 model. More recently, Kawasaki and Kotsuki (2024) introduced the model predictive control (MPC) within the CSE and applied it to controlling the Lorenz 63 model (see also a paper by Nagai et al. (2024)). However, control methods such as the MPC are computationally expensive. The computational cost of determining the optimal inputs can bottleneck practical applications of high-dimensional dynamical systems such as numerical weather predictions models. To overcome this bottleneck, Sawada (2024a, b) introduced an ensemble Kalman filter–based control method, which efficiently finds local and intermittent interventions, and applies it to controlling the Lorenz 63 and 96 models.

Following these previous works, we investigate a mathematical algorithm that mitigates extreme events, using the Lorenz 96 model as a testbed. Practical weather control applications must be feasibly implementable. Given the large scales of weather systems and the limited energy available for control, interventions will be typically constrained to local sites and specific time-points (Sawada, 2024b). The Lorenz 96 model is a minimal mathematical system for investigating feasible control strategies in spatially extended chaotic systems (Lorenz, 1996; Sun et al., 2023; Sawada, 2024b). Sun et al. (2023) proposed a method for mitigating extreme events in the Lorenz 96 model. Their method is primarily designed to apply control inputs across all grid variables. When control is limited to a single site, at least in a specific setting, the success rate of their method declines to approximately 60%. To improve the results of Sun et al. (2023), we propose a new methodology that identifies effective local interventions.

Control-theoretic methods such as MPC are top–down approaches that compute optimal control inputs by minimizing a cost function subject to given constraints (Kawasaki and Kotsuki, 2024; Nagai et al., 2024; Ohtsuka et al., 2024). In contrast, the present study pursues a bottom–up approach to mitigate extreme events using a finite set of available intervention options. We assume that the number of available options for human intervention in weather will remain limited for the foreseeable future, given the time required for technological advancements. Hence, we generate ensemble forecasts for a limited set of local intervention scenarios and implement the most effective intervention based on these forecasts. To account for the chaotic uncertainty in predictions, the selection of the "best" scenario is updated over time. The large number of potential intervention scenarios is reduced to a manageable subset to ensure computational feasibility. Despite this constraint, our method mitigates extreme events in the Lorenz 96 model with higher success rates than the method of Sun et al. (2023).

The remainder of this article is organized as follows. The Lorenz 96 model, the local ensemble transform Kalman filter (LETKF)-based data assimilation method, and our control algorithm for extreme events are explained in Sections 2.1–2.3, respectively. Section 3 presents the results, and Section 4 discusses the limitations and potential extensions of our method. We

https://doi.org/10.5194/egusphere-2025-987
Preprint. Discussion started: 21 March 2025

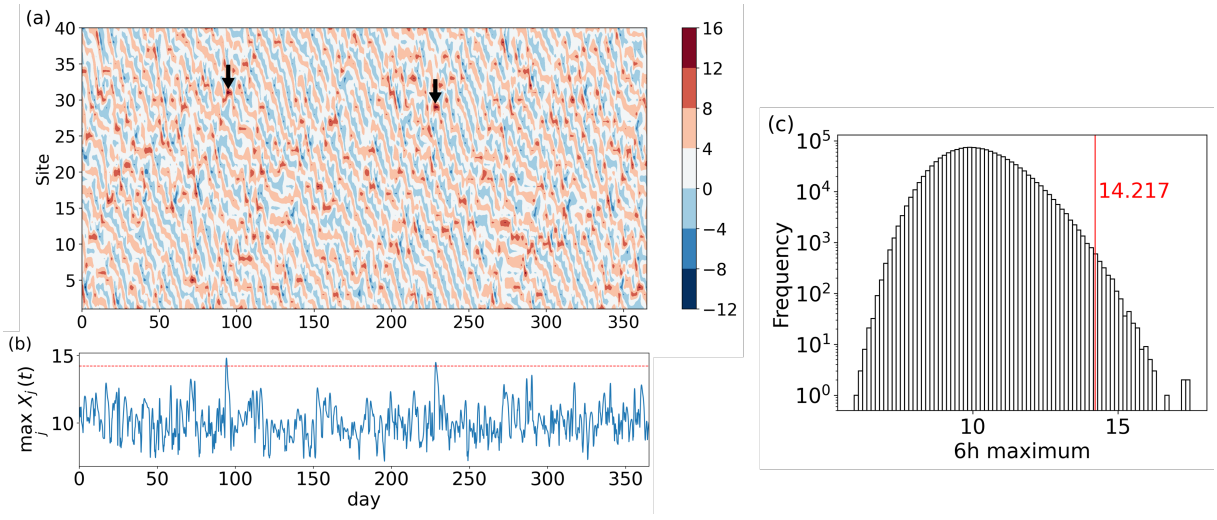

Figure 1. Extreme events in the Lorenz 96 model: (a) spatiotemporal variations of $X_j(t)$ over 365 d. The two arrows indicate extreme events exceeding the threshold value 14.217. (b) Time series of the maximum value across 40 sites at each time step. The horizontal red line represents the threshold 14.217. (c) Histogram of 6-h maxima, representing the maximum X-values across all the sites within each 6-h period.

also highlight the similarity between our method and the so-called rare event algorithms, which efficiently simulate events with extremely low probabilities (Ragone et al., 2018; Wouters et al., 2023; Cini et al., 2024; Sauer et al., 2024).

2 Methods

2.1 Lorenz 96 model and extreme events

The toy model of weather systems proposed by Lorenz (1996) contains J variables, X_1, ..., X_J and is governed by

$$\frac{dX_j}{dt} = (X_{j+1} - X_{j-2})X_{j-1} - X_j + F,$$

where F is a constant parameter. Periodic boundary conditions $X_{J-1} = X_{-1}$, $X_J = X_0$, $X_{J+1} = X_1$ are assumed. The variables X_j can be interpreted as unspecified meteorological quantities measured along a circle of constant latitude of the Earth. For common parameter values $J = 40$ and $F = 8$ (Lorenz and Emanuel, 1998), the dynamics are chaotic (Fig. 1a). The time unit is commonly assumed as 5 days (d) (Lorenz and Emanuel, 1998). The error doubling time of the Lorenz 96 model is then comparable to those of modern General Circulation Models. The Lorenz 96 equation is integrated using the forth-order Runge–Kutta method with a time step of $\Delta t = 0.01$ corresponding to 1.2 hours (h).

The Lorenz 96 model exhibits sporadic "extreme events" characterized by very high values. The method of Sun et al. (2023) aims to prevent values of the variable X_j above a threshold of 14.217. On average, the maximum values across all the sites during each 6-h period (hereafter referred to as the *6-h maxima*) will exceed the threshold twice per year (Figs. 1a and b).

https://doi.org/10.5194/egusphere-2025-987
Preprint. Discussion started: 21 March 2025

Herein, we adopt the same threshold (14.217) to enable a straightforward comparison between our results and theirs. The histogram of 6-h maxima is shown in Fig. 1c.

2.2 Data assimilation method

Data assimilation combines model simulations and noisy observations to estimate the state of a dynamical system. Data assimilation is essential in weather forecasting and was thus employed in previous weather control studies. Following a paper by Sun et al. (2023), our data assimilation method uses the LETKF, a variant of the Ensemble Kalman Filter that enhances the computational efficiency and scalability in high-dimensional systems (Hunt et al., 2007).

Herein, we briefly outline the LETKF (Hunt et al., 2007; Kotsuki and Bishop, 2022). Consider a dynamical systems model providing ensemble forecasts $\{\boldsymbol{x}^{b(i)}\}_{i=1}^{m}$, where m is the number of ensemble members and the suffix b stands for background or forecast. The LETKF transforms the ensemble forecasts $\{\boldsymbol{x}^{b(i)}\}_{i=1}^{m}$ into an *analysis ensemble* $\{\boldsymbol{x}^{a(i)}\}_{i=1}^{m}$, whose mean $\overline{\boldsymbol{x}^a}$ minimizes the following cost function:

$$J(\boldsymbol{x}) = (\boldsymbol{x} - \overline{\boldsymbol{x}^b})^T (\boldsymbol{P}^b)^{-1} (\boldsymbol{x} - \overline{\boldsymbol{x}^b}) + (\boldsymbol{y} - H(\boldsymbol{x}))^T \boldsymbol{R}^{-1} (\boldsymbol{y} - H(\boldsymbol{x})),$$

where $\overline{\boldsymbol{x}^b}$ is the forecast mean, $\boldsymbol{P}^b$ is the forecast-error covariance matrix, $\boldsymbol{y}$ and H denote the observation vector and observation operator, respectively, and $\boldsymbol{R}$ is the observational-error covariance matrix (here assumed as diagonal). The first term in $J(\boldsymbol{x})$ penalizes deviations of the analysis mean from the forecast, weighted by the confidence in the forecast. The second term penalizes deviations from the observations, weighted by the confidence in the observations.

The LETKF optimizes the cost function $J(\boldsymbol{x})$ through an ensemble-based approach and localization principles. The background error covariance is approximated as $\boldsymbol{P}^b \approx \frac{1}{m-1} \boldsymbol{X}^b (\boldsymbol{X}^b)^T$, where $\boldsymbol{X}^b$ is the matrix of background ensemble perturbations with the i-th column given by $\boldsymbol{x}^{b(i)} - \overline{\boldsymbol{x}^b}$. Equivalently, this expression can be written as $\boldsymbol{P}^b \approx \boldsymbol{Z}^b (\boldsymbol{Z}^b)^T$, where $\boldsymbol{Z}^b = \boldsymbol{X}^b / \sqrt{m-1}$. Based on observations, the analysis ensemble is updated in the reduced-dimensional subspace spanned by $\boldsymbol{Z}^b$. In particular, the LETKF updates the analysis on a grid by grid basis as

$$\begin{aligned} \boldsymbol{X}^a &= \overline{\boldsymbol{x}^b} \cdot \boldsymbol{1} + \boldsymbol{Z}^b \boldsymbol{T}, \\ \boldsymbol{T} &= \tilde{\boldsymbol{P}}^a (\boldsymbol{Y}^b)^T \boldsymbol{R}_{\text{loc}}^{-1} (\boldsymbol{y} - H(\overline{\boldsymbol{x}^b})) \cdot \boldsymbol{1} + \sqrt{m-1} (\tilde{\boldsymbol{P}}^a)^{1/2}. \end{aligned}$$

Here, $\boldsymbol{1}$ is a row vector of ones, and $\boldsymbol{Y}^b \approx (H(\boldsymbol{X}^b) - \overline{H(\boldsymbol{X}^b)} \cdot \boldsymbol{1}) / \sqrt{m-1}$. The matrix $\tilde{\boldsymbol{P}}^a$ is derived as $\tilde{\boldsymbol{P}}^a = \boldsymbol{\Lambda} \boldsymbol{D}^{-1} \boldsymbol{\Lambda}^T$ from eigenvalue decomposition $(\tilde{\boldsymbol{P}}^a)^{-1} = \boldsymbol{I} + (\boldsymbol{Y}^b)^T \boldsymbol{R}_{\text{loc}}^{-1} \boldsymbol{Y}^b = \boldsymbol{\Lambda} \boldsymbol{D} \boldsymbol{\Lambda}^T$. Further, the square root of $\tilde{\boldsymbol{P}}^a$ is given as $(\tilde{\boldsymbol{P}}^a)^{1/2} = \boldsymbol{\Lambda} \boldsymbol{D}^{-1/2} \boldsymbol{\Lambda}^T$. The matrix $\boldsymbol{R}_{\text{loc}}$ is the localized observation-error covariance, which is also diagonal. When updating at each grid point j, the i-th diagonal element of $\boldsymbol{R}_{\text{loc}}^{-1}$ is defined as $(\boldsymbol{R}^{-1})_{ii} \exp\left(-\frac{|i-j|^2}{2\sigma^2}\right)$ if $|i-j| < 2\sqrt{\frac{10}{3}}\sigma$ and zero otherwise. Here, σ is the localization parameter. Localizing updates to relevant regions reduces the impact of spurious correlations in covariance estimates. At site j, only the j-th row of the analysis ensemble $\boldsymbol{X}^a$ is used in subsequent forecasts. Error covariance underestimation is handled by a multiplicative covariance inflation as $\boldsymbol{X}^b \leftarrow \rho \boldsymbol{X}^b$, where $\rho > 1$ is the inflation coefficient (Kotsuki and Bishop, 2022).

https://doi.org/10.5194/egusphere-2025-987
Preprint. Discussion started: 21 March 2025

Following a paper by Sun et al. (2023), we observe the system at 6-h intervals (i.e., at every five time steps with $\Delta t = 0.01$). The observation is modeled as $y_j(t) = H(X_j(t)) + \varepsilon_j(t)$, where $\varepsilon_j(t)$ is independent white Gaussian noise with zero mean and unit standard deviation. The linear observation operator $H(X_j) = X_j$ is assumed at all 40 sites unless otherwise stated (partial observations are considered in Section 3.4). Every 6 h, having obtained the observations $\boldsymbol{y}$, we assimilate the data using the LETKF to obtain the analysis ensemble $\{\boldsymbol{x}^{a(i)}\}_{i=1}^{m}$, providing the initial condition of subsequent ensemble forecasts (cf. Fig. 2b(i)). Unless otherwise stated, we set $m = 10$, $\sigma = 6.0$, $\rho = 1.03$, and $\boldsymbol{R}$ as the identity matrix. Applying LETKF with these parameters, the root mean square error between the analysis mean and the true state is 0.1973, comparable to that of Sun et al. (2023) (0.1989).

2.3 Intervention method for reducing extreme events

To mitigate extreme events in the Lorenz 96 model, we introduce an intervention input $\boldsymbol{u}(t) = (u_1(t), u_2(t), ..., u_N(t))^T$ into the system as

$$\frac{dX_j}{dt} = (X_{j+1} - X_{j-2})X_{j-1} - X_j + F - u_j(t). \tag{1}$$

The sign preceding $u_j(t)$ is negative by default. To identify effective intervention inputs, we perform ensemble forecasts assuming several sequences of intervention inputs $\boldsymbol{u}(t)$ called *intervention scenarios* (Fig. 2a). The *intervention-off scenario* planned at time s is given by

$$u_i(t) = u_i(s) \text{ for } s \le t < s + 6\,\text{h}, \text{ and } u_i(t) = 0 \text{ for } t \ge s + 6\,\text{h}. \tag{2}$$

The *one-site intervention scenario* at site j planned at time s is given by

$$u_i(t) = u_i(s) \text{ for } s \le t < s + 6\,\text{h}, \text{ and } u_i(t) = \begin{cases} u & \text{if } i = j, \\ 0 & \text{if } i \ne j \end{cases} \text{ for } t \ge s + 6\,\text{h}. \tag{3}$$

Notably, the actual input size u is nonzero only at site j. The 6-h interval $s \le t < s + 6$ h corresponds to the period between successive observations, during which the input remains constant at its value $\boldsymbol{u}(s)$ determined in the previous 6-h interval. Within each 6-h interval, we evaluate intervention scenarios implemented after 6 h. Variants of the one-site intervention scenarios are introduced in Sections 3.2 and 3.3.

We now outline our method for reducing extreme events (Fig. 2). The implementation steps of the method are given in Appendix A. At 6-h intervals, we observe the system and update the analysis ensemble using the LETKF (Fig. 2b(i)). The updated analysis ensemble becomes the initial conditions of the risk assessment (Fig. 2b(ii)) and multi-scenario ensemble forecasts (Fig. 2b(iii)) during the following 6 h. The next observations are then obtained (see below). From the start of the subsequent 6-h cycle, we implement the new scenario in the operations.

Risk assessment. To avoid unnecessary interventions in the system, we preassess the risk of extreme events through a T-d ensemble forecast from the latest analysis ensemble under the intervention-off scenario (Fig. 2b(ii)). Focusing on a prediction horizon of $T = 7$ d, we examine the dependence of the success rate on T. A binary flag "ALERT" signals the need for control

https://doi.org/10.5194/egusphere-2025-987
Preprint. Discussion started: 21 March 2025

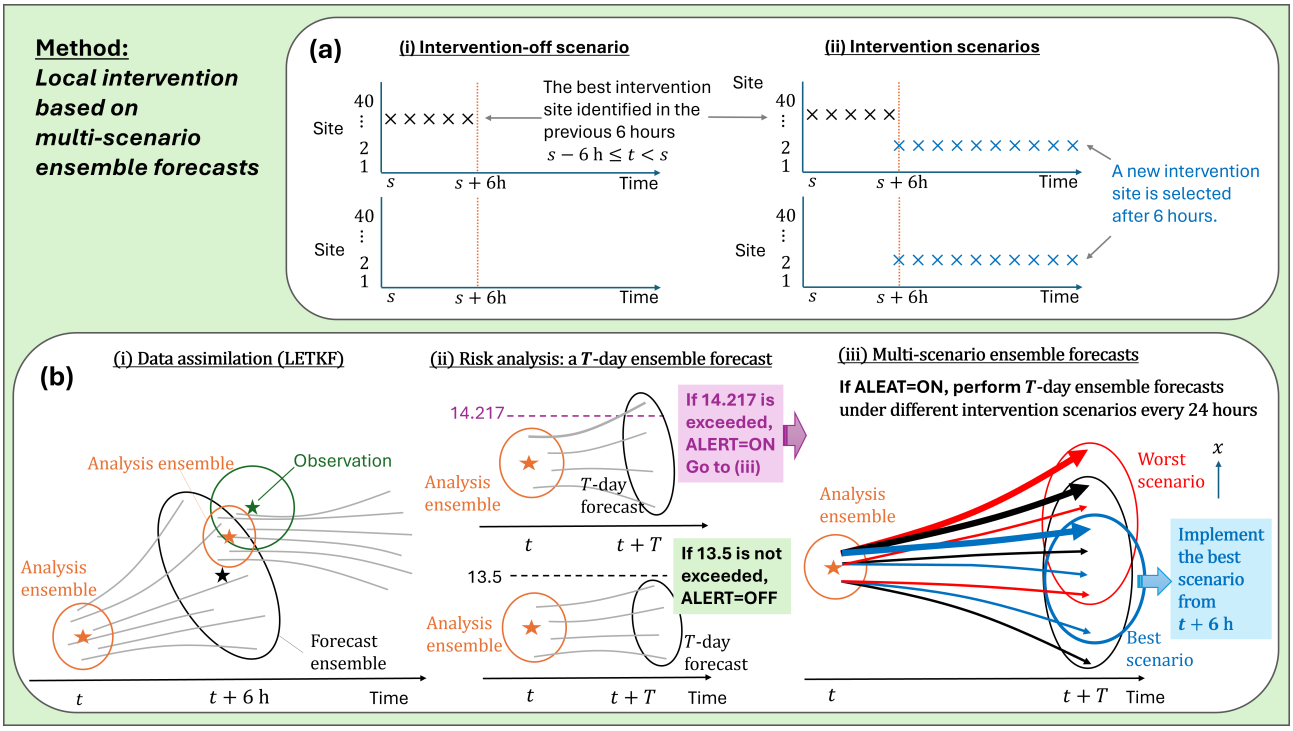

Figure 2. Method for reducing extreme events. (a) Intervention-off scenario and intervention scenarios at 40 possible intervention sites. Each cross mark ("×") indicates the addition of a nonzero input at one of the 40 sites at each time step. In the intervention-off scenario (a-i), any intervention is switched off after 6 h. In an intervention scenario (a-ii), a new intervention site is selected after 6 h. (b) Key steps of the method: (b-i) data assimilation using the LETKF, (b-ii) risk assessment of a T-d ensemble forecast under the intervention-off scenario, and (b-iii) multi-scenario ensemble forecasts and interventions. Under the best scenario (blue), the worst member in the T-d ensemble forecast (thick arrow) is most effectively mitigated. See text for details.

operations. If ALERT = OFF and an extreme event exceeding the upper threshold 14.217 is predicted within T d in any ensemble member, we set ALERT = ON. If ALERT = ON and the maximum value across all the ensemble members within T d is below the lower threshold 13.5, we set ALERT = OFF. Otherwise the flag is unchanged.

multi-scenario ensemble forecasts and local intervention. The action taken depends on the risk assessment result. If ALERT = OFF, we operate the intervention-off scenario given by Eqs. (1) and (2) in both the nature run and the ensemble forecast in the data assimilation using the LETKF. If ALERT = ON, we perform T-d ensemble forecasts under possible intervention scenarios (Fig. 2b(iii)). These multi-scenario ensemble forecasts are conducted less frequently (at 24-h intervals) than the 6-h data assimilation because multi-scenario ensemble forecasts are computationally expensive and the forecast results change relatively infrequently. When planning a one-site intervention among the 40 sites, 400 forecasts with different combinations of 10 ensemble members and 40 intervention scenarios (i.e., sites) are performed. In each scenario, we obtain 10 outcomes corresponding to the 10 ensemble members. From the perspective of risk hedging, we assume that the best intervention scenario

https://doi.org/10.5194/egusphere-2025-987
Preprint. Discussion started: 21 March 2025

minimizes the maximum value across all the sites and ensemble members over the next T d. Other criteria, such as minimizing the expected maximum among ensemble members, are also possible. If any intervention scenario with nonzero u cannot reduce the maximum from that of the intervention-off scenario, the intervention-off scenario becomes the best scenario. The selected best scenario is then operated from the next 6-h cycle.

3 Results

This section presents the CSE results of our method. A single CSE spans 1010 years (y). Transients are eliminated by excluding the first 10 y, and analysis is performed by dividing the subsequent 1000 y (730,000 steps) into ten 100-y segments. The performance scores are assessed in each segment, and the standard deviations of the scores are represented as error bars in the corresponding figures. As the error doubling time is 0.42 units, i.e., 42 steps, the segments are effectively independent. Following Sun et al. (2023), the simulation run controlled by intervention inputs is called the *controlled nature run*.

Our control strategies are evaluated in terms of three metrics. The first metric is the *success rate*, defined as follows (Sun et al., 2023):

$$\text{success rate} = 1 - \frac{\text{(number of 6-h intervals in 100 y with extreme events)}}{200}.$$

Here, the denominator is set to 200 because two extreme events per year are expected at a threshold of 14.217. Alternatively, the success rate can be defined by the ratio of extreme event frequencies with and without control, but both definitions yield nearly identical results. The second metric is the *intervention energy* defined by the sum of displacement norms induced by intervention inputs (Sun et al., 2023). It is mathematically written as $\sum_t \|\boldsymbol{X}_{\text{intervened}}(t+\Delta t) - \boldsymbol{X}_{\text{unintervened}}(t+\Delta t)\|$, where $\boldsymbol{X}_{\text{intervened}}(t+\Delta t)$ and $\boldsymbol{X}_{\text{unintervened}}(t+\Delta t)$ are one-step-ahead values for the cases with and without intervention inputs, respectively, both computed from the controlled nature run $\boldsymbol{X}_{\text{intervention}}(t)$. For one-site intervention, this metric is roughly estimated as

$$\text{intervention energy} \approx u\Delta t \times \text{(number of steps with nonzero intervention)}.$$

The third metric is the *number of scenario changes*. It measures the frequency of changes in the control input vector, $\boldsymbol{u}(t)$, per year in the controlled nature run, serving as a measure of operational cost. This metric is particularly relevant when implementing interventions by static obstacles requiring no energy postplacement.

3.1 One-site intervention among 40 sites

First, we consider the simplest intervention case at a single site among the 40 sites at each time step. Figure 3 presents an example snapshot of the CSE with a prediction horizon of $T = 7$ d. An extreme event exceeding the 14.217 threshold is detected in the 7-d ensemble forecast conducted at $t = 123$, triggering ALERT = ON (Fig. 3a). Next, 7-d ensemble forecasts are performed in 40 scenarios at different intervention sites (Fig. 3b). The intervention at site 35 most effectively minimized the maximum across the sites and ensemble members over the ensuing 7 d. Therefore, the intervention at site 35 is implemented

https://doi.org/10.5194/egusphere-2025-987
Preprint. Discussion started: 21 March 2025

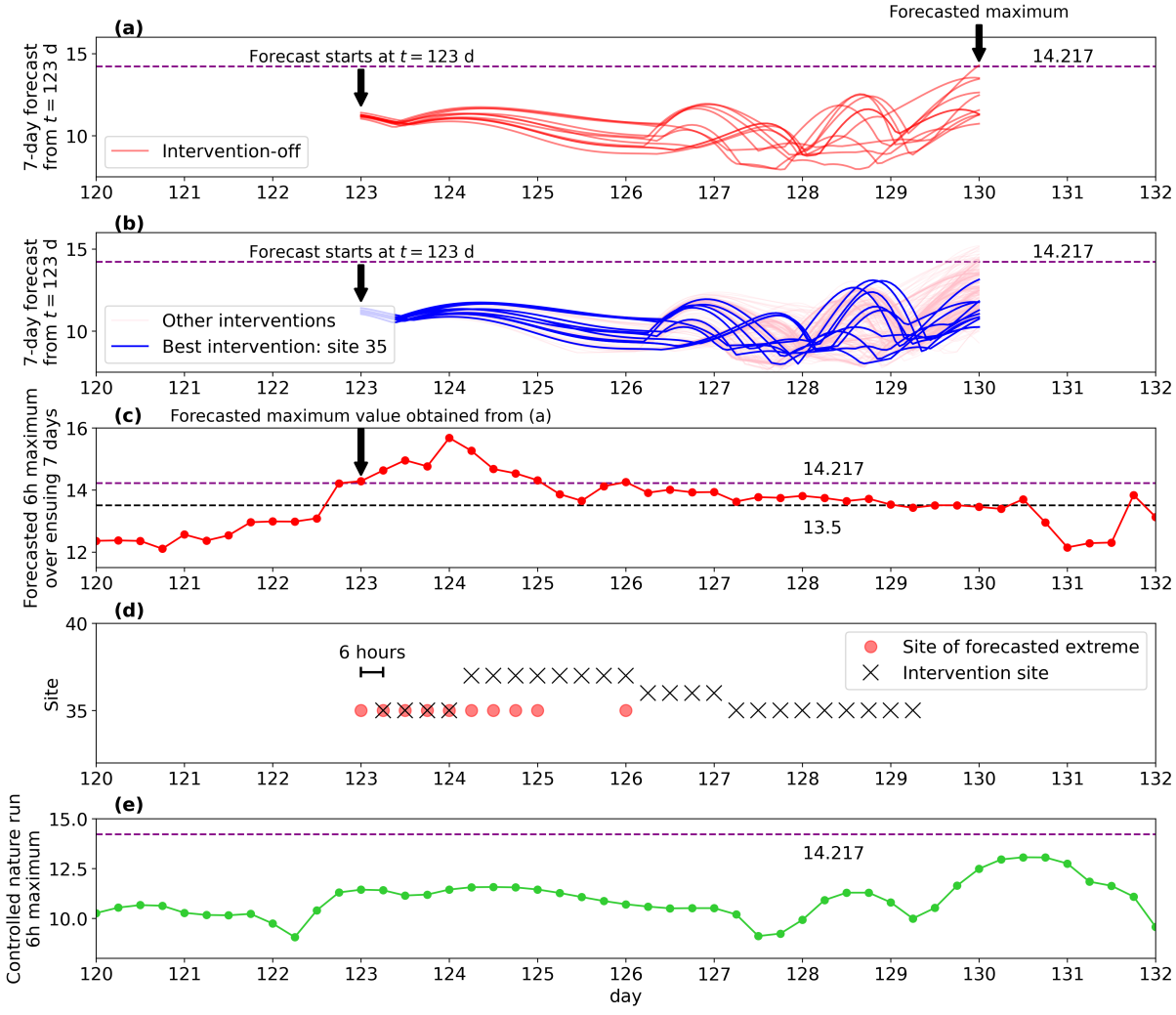

Figure 3. A snapshot of the CSE with input size $u = 1$ and prediction horizon $T = 7$ d: (a) 7-d forecast from day 123 under the intervention-off scenario. The 10 lines represent the time evolution of the maximum values across the 40 sites, $\max_{1 \le j \le 40} \tilde{X}_j(t)$, for each of the 10 ensemble members. As one ensemble member crosses the threshold 14.217, ALERT is set to ON. (b) Same as (a) but for 40 different intervention scenarios. The best scenario is the intervention at site 35 (blue). (c) Forecasted 6-h maximum over the ensuing 7 d. Each point is plotted at the time of forecasting. (d) Sites of forecasted extremes (red circles) and interventions (crosses) during each 6-h cycle. Note that the actual intervention is implemented 6 h after the forecast, and the optimal intervention site is updated at 24 h intervals. (e) Controlled nature run, successfully maintained below the threshold of 14.217.

175 from the next 6-h cycle (Fig. 3d). The operations are performed at 6-h intervals as described in Methods. The 6-h maxima of the controlled nature run (blue) were successfully maintained below the upper threshold of 14.217 (Fig. 3e).

https://doi.org/10.5194/egusphere-2025-987
Preprint. Discussion started: 21 March 2025

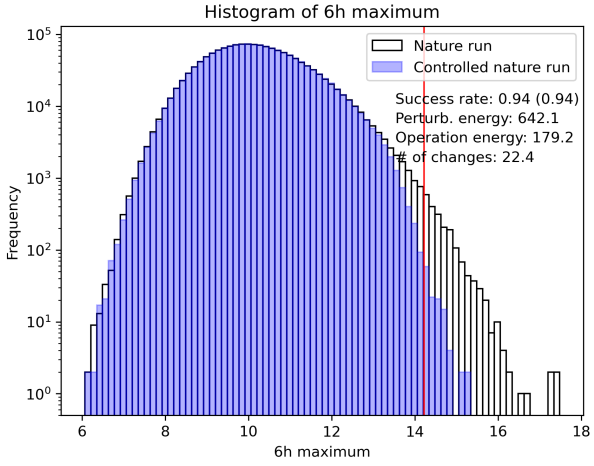

Figure 4. CSE result of intervening at a single site among 40 sites. Plotted are histograms of the 6-h maxima during the controlled (blue) and uncontrolled (white) nature runs. The input size u is 1.6. The vertical red line represents the 14.217 threshold below which the state variables are intended to be maintained. The success rate is 94.2%.

Figure 4 compares the histograms of 6-h maxima in the controlled and uncontrolled nature run for an input size of $u = 1.6$ and a prediction horizon of $T = 7$ d. The extreme events are mitigated at a success rate of 94%, largely exceeding the 60% success rate achieved by Sun et al. (2023) at specific settings of 4 d for the prediction horizon and 0.7 for the perturbation-size coefficient α. Maintaining $T = 7$ d, the success rate initially increases with increasing input size u and eventually saturates at around 94% when u exceeds ~ 1.6 (Fig. 5a). However, increasing the input size u increases the required intervention energy because a larger force induces a greater displacement of the state, highlighting a success–cost trade-off. At $u \gtrsim 0.5$, the intervention energy is larger in our method than in the method by Sun et al. (2023) but does not exceed three times the earlier value (Fig. 5b). Fortunately, the number of scenario changes decreases with increasing input size u, reflecting the corresponding magnitude increase of the interventions (Fig. 5c). The frequency of scenario changes is reasonably small (20–27 per year).

Next, the performance dependence on the prediction horizon T was examined for a fixed input size u. Increasing the prediction horizon T generally increases the success rate (Fig. 6a) but disadvantageably increases both the intervention energy and number of scenario changes (Figs. 6b and c), again highlighting the success–cost trade-off.

3.2 One-site intervention near the predicted extreme

Whether interventions across all 40 sites are feasible or (if feasible) necessary is not guaranteed. Therefore, we restrict interventions to the vicinity of the site of a predicted extreme event under the intervention-off scenario. Figure 7 plots the three control-performance measures for different numbers of neighboring sites where interventions are allowed $\{1, 3, 7, 11, 21, 31, 40\}$. Interestingly, the success rate is maximized when the neighborhood size is 21, approximately half the total number of sites,

https://doi.org/10.5194/egusphere-2025-987
Preprint. Discussion started: 21 March 2025

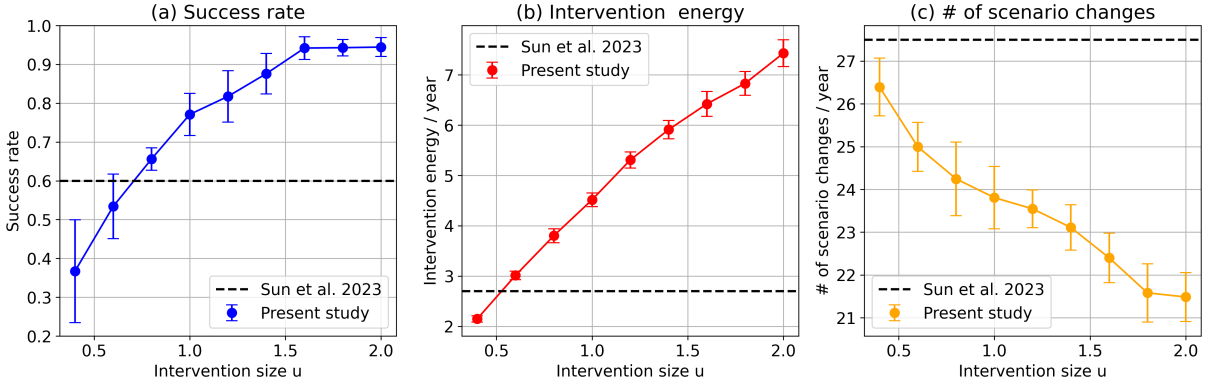

Figure 5. Performance metrics versus input size u of the proposed control method at a single intervention site: (a) success rate, (b) intervention energy, and (c) number of scenario changes. The prediction horizon T is 7 d. Error bars represent one standard deviation among 10 experimental results under different initial conditions. The horizontal dashed lines show the reference scores obtained under a specific setting in the work by Sun et al. (2023).

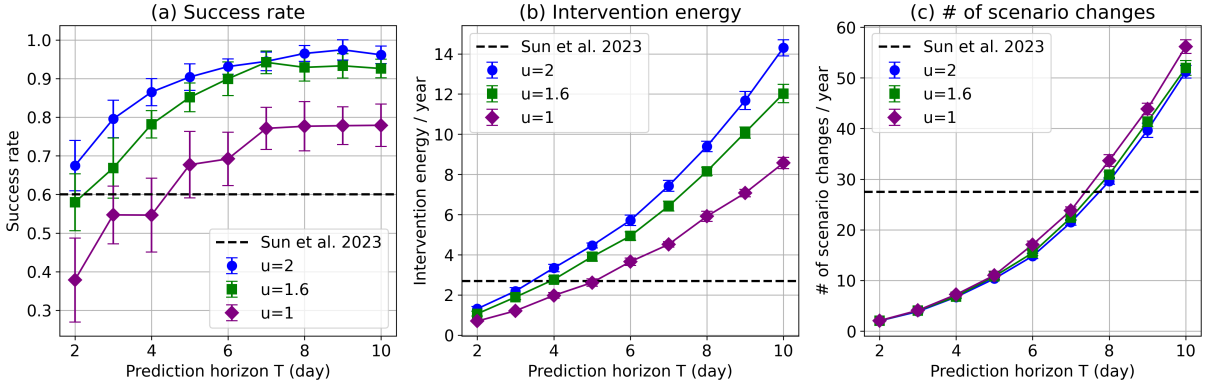

Figure 6. Performance metrics versus prediction horizon T of the proposed control method at a single intervention site: (a) success rate, (b) intervention energy, and (c) number of scenario changes. Results are shown for different input sizes $u = 1$, 1.6, and 2. The horizontal dashed lines are the reference scores obtained under a specific setting in the work by Sun et al. (2023).

From this result, we inferred that restricting the number of intervention sites prevents ineffective interventions at sites far from the extreme event.

3.3 Two-site intervention in the vicinity of a predicted extreme

The previous subsections were limited to single-site interventions. This subsection analyze the outcomes of intervention at two sites. Figure 8 shows the CSE results in a case with at most two intervention sites among 11 self-inclusive neighbors. The total number of possible scenarios is 67, comprising $\binom{11}{2}$ combinations of two intervention sites, 11 single-site interventions,

https://doi.org/10.5194/egusphere-2025-987
Preprint. Discussion started: 21 March 2025

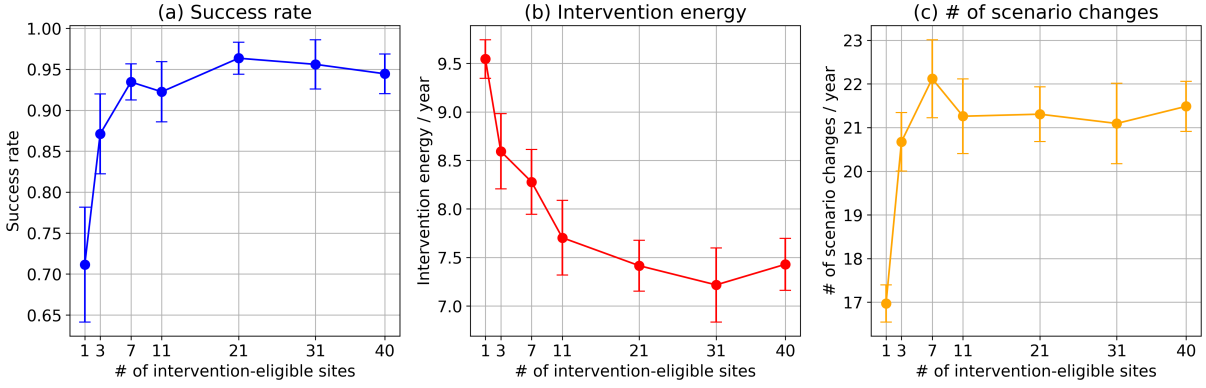

Figure 7. Performance of the proposed control method versus number of intervention-eligible sites at a single intervention site: (a) Success rate, (b) intervention energy, and (c) number of scenario changes. $u = 2$ and $T = 7$ d.

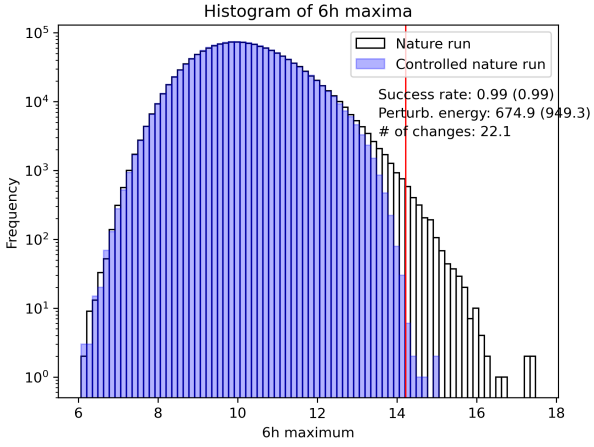

Figure 8. CSE result of intervening at two sites near a predicted weather extreme. Plotted are histograms of 6-h maxima during the controlled natural (blue) and uncontrolled (white) nature runs with $u = 2.0$ and $T = 7$ d. The vertical red line represents the 14.217 threshold below which the state variables are intended to be maintained. The success rate is 99.4%.

and the no-intervention scenario. The success rate reaches 99.4%. Surprisingly, only a slight increase in the input dimensions efficiently improves the control performance.

Next, we examine the sensitivity of the results to number of intervention-eligible sites (Fig. 9). The success rate remains at 98%–99% when the number of intervention-eligible sites is five or higher and remains high (92.7%) when the eligible-site number declines to three. Meanwhile, the interaction energy of multisite intervention increases by only around 15%–25% from that of single-site interaction (compare Fig. 9 with Fig. 7).

https://doi.org/10.5194/egusphere-2025-987
Preprint. Discussion started: 21 March 2025

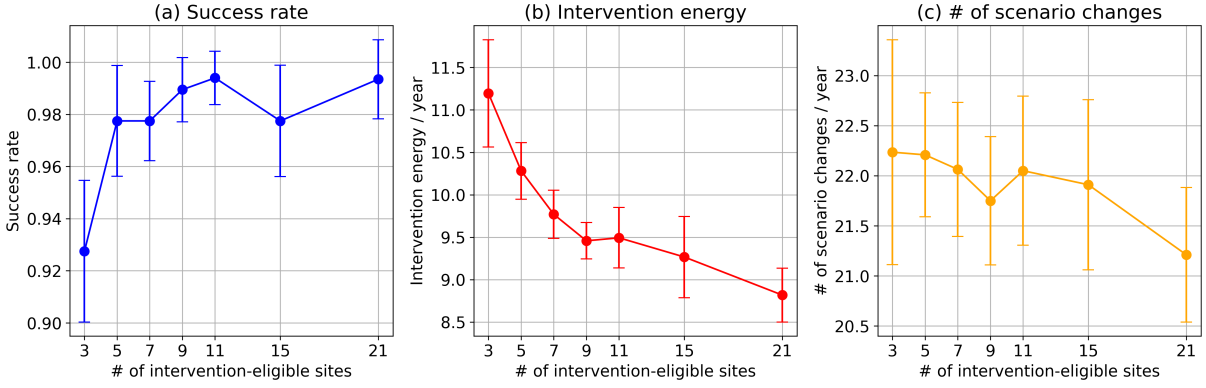

Figure 9. Performance metrics of the proposed control method with two intervention sites versus number of intervention-eligible sites: (a) success rate, (b) intervention energy, and (c) number of scenario changes. $u = 2$ and $T = 7$ d.

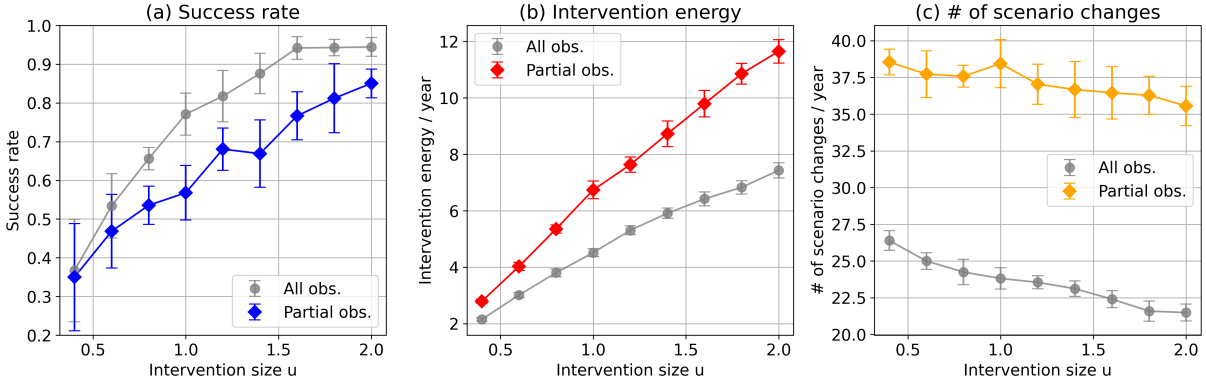

Figure 10. Comparison of performance metrics versus input size u in cases of full and partial observations during single-site intervention among 40 sites: (a) success rate, (b) intervention energy, and (c) number of scenario changes. $T = 7$ d.

3.4 Partial observation

In real-world applications, complete observations of all state variables are often lacking. Therefore, this section investigates the performance of our method under partial observations. Following the researches by Sun et al. (2023) and Sawada (2024b), we assume that the state of the system can be observed at 20 sites with odd indices.

We first consider eligible intervention at a single site among 40 sites. Figure 10 compares the performance results of the partial and complate observations as functions of input size u. Partial observations decrease the success rate by 26% at most over $0 \leq u \leq 2$, while increasing the intervention energy and number of scenario changes by 57% and 68% at most, respectively.

Second, we compare the performance results of partial and full observations when intervening at two sites among the 40 sites. Figure 10 plots the results as functions of number of intervention-eligible sites at $u = 2$. In the partial-observation case, the

https://doi.org/10.5194/egusphere-2025-987
Preprint. Discussion started: 21 March 2025

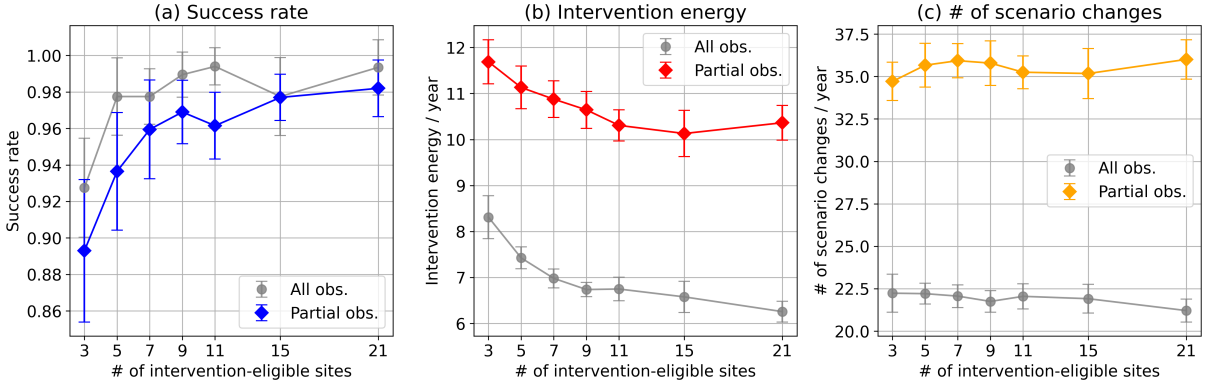

Figure 11. Comparison of performance metrics versus number of intervention-eligible sites in cases of full and partial observations during two-site interventions among 40 sites: (a) success rate, (b) intervention energy, and (c) number of scenario changes. $u = 2$ and $T = 7$ d. In the partial-observation case, the LETKF parameters are slightly re-tuned to improve the performance. The localization length scale is $\sigma = 5.9$ and the number of ensemble members is $m = 11$.

LETKF parameters were slightly re-tuned to improve the performance. The localization length scale and number of ensemble members were set to $\sigma = 5.9$ and $m = 11$, respectively. Partial observations decrease the success rate by a small fraction (only 0%–4%) from that of complete observations (Fig. 11a), but increase the intervention energy and number of annual scenario changes (Figs. 11b and c). Therefore, the present method handles partial observations with a high success rate but incurs higher control costs.

4 Summary and discussions

Herein, we proposed a bottom–up approach that reduces the number of extreme events in the Lorenz 96 model with limited intervention options. Alongside data assimilation, we performed T-d ensemble forecasts under the intervention-off scenario. When the T-d ensemble forecasts included an extreme event, we explored the best scenario that maximally mitigated the highest extreme value produced by the ensemble members through multi-scenario ensemble forecasts. We then implemented the identified best scenario. The success rate of our method was approximately 94% when perturbing one site per step and 99.4% when perturbing two sites per step. Our method improved the success rate of Sun et al. (2023) (∼60% obtained under a specific setting) by approximately 34%, while increasing the intervention energy requirement by only a few times. Several factors may contribute to this significant improvement. In Sun et al. (2023), the perturbation is scaled between the worst and best trajectories, meaning that the control input is not optimized. In contrast, our method selects the optimal intervention scenario from the available options. It is also worth noting that their reported success rate of approximately 60% may not be fully optimized with respect to the chosen parameters.

In addition to its high success rate, our method also exhibited robustness to missing observations, achieving high success rates even when half of the observations were unavailable (Fig. 11). Sensitivity analyses varying the method parameters revealed

https://doi.org/10.5194/egusphere-2025-987
Preprint. Discussion started: 21 March 2025

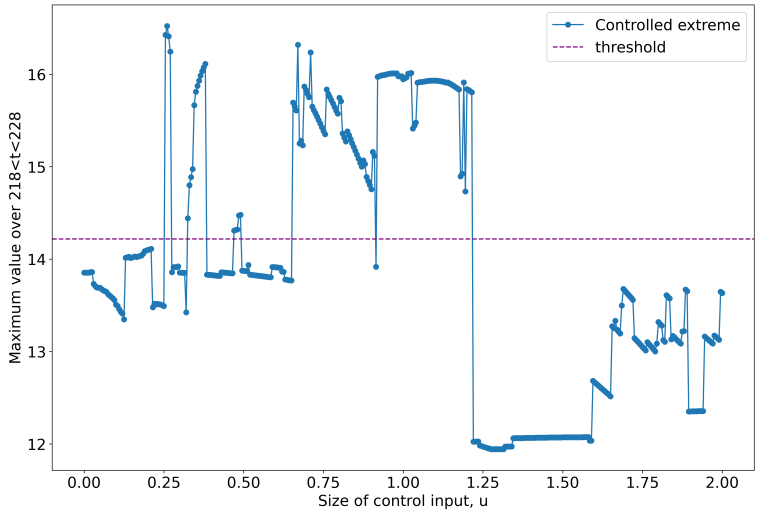

Figure 12. Sensitivity of the present control method to size of the control input u. Plotted is the 6-h maximum of the controlled nature run over a certain time horizon $218 < t < 228$ as a function of u. The extreme value largely depends on u, especially between $u = 1.21$ and $u = 1.22$. The dashed line represents the 14.217 threshold.

the success–cost trade-off. In the actual implementation, the parameters should be chosen to maximize the success rate while adhering to constraints on intervention energy, the number of scenario changes per year, and other relevant factors. Interestingly, both the maximization of the success rate and the minimization of intervention energy were achieved at an intermediate number of intervention-eligible sites (Fig. 7). Limiting these sites not only helps avoid ineffective interventions but also reduces the computational cost of optimizing the intervention scenario.

The success rate of the method rather smoothly changes with the intervention size u (Figs. 5 and 10). However, when mitigating each extreme event, the success of mitigation can strongly depend on the input size u. To demonstrate the sensitivity to u, Fig. 12 plots the extreme value observed over a certain time interval as a function of u in an extreme-event instance. The maximum value drastically changes between $u = 1.21$ and $u = 1.22$ because the best intervention sites differ between the two cases, and this difference leads to different trajectory evolutions. Therefore, even if controlling an extreme event is predicted to fail at a particular value of the input size u, successful control may be achieved with a slight additional increase of u. This complex behavior arises from the interplay between algorithmic thresholds and nonlinear trajectory evolutions.

Our current approach identifies the best scenario among multiple candidates through a brute-force grid search, which limits the number of evaluable scenarios. To overcome this limitation, optimization techniques such as Bayesian optimization, genetic algorithms, and particle swarm optimization, which can efficiently identify effective intervention scenarios, will be explored in future work. Moreover, recent artificial-intelligence-based weather prediction models may enlarge the number of potential intervention scenarios (Price et al., 2025; Kotsuki et al., 2024).

Our control method is analogous to rare event simulation (RES), which simulates rare events with probabilities too small to be sampled through standard Monte Carlo simulations (Ragone et al., 2018; Wouters et al., 2023; Cini et al., 2024; Sauer

https://doi.org/10.5194/egusphere-2025-987
Preprint. Discussion started: 21 March 2025

et al., 2024). A type of RES called the genealogical particle analysis (Del Moral and Garnier, 2005) generates multiple system trajectories with small, naturally occurring perturbations (mutations) that preserve the statistical properties of the system. A subset of trajectories that approach the target event is selected and replicated with appropriate weights while all others are terminated (selection). By iterating the mutation and selection processes, this RES efficiently simulates rare events and estimates their true probabilities based on the number of simulated rare events adjusted by the assigned weights. The mutation and selection processes in RES are similar to our multi-scenario ensemble forecasts and the selection of intervention scenarios, respectively. In fact, our method was inspired by the RES framework, which obtains a rare event through a sequence of small perturbations. Analogously, our bottom–up approach mitigates extreme events through a sequence of limited intervention options.

At present, our work is a proof of concepts demonstrated on a toy model of weather systems. The method should be tested in higher-dimensional models such as realistic numerical weather models and in situations with model uncertainty.

Code availability. The codes used in this study will be uploaded to a repository following acceptance of the paper.

Appendix A: Step-by-step description of the control simulation experiment

The following operations are performed at 6-h intervals.

1. At time s, we have the analysis ensemble $\{\boldsymbol{x}^{a(i)}(s)|\, i = 1, ..., m\}$ with m members (e.g., $m = 10$). Starting from $\{\boldsymbol{x}^{a(i)}(s)|\, i = 1, ..., m\}$ with the input $\boldsymbol{u}(t)$ planned in the previous 6-h interval, we integrate Eq. (1) to obtain the background ensemble $\{\boldsymbol{x}^{b(i)}(s + 6\,\mathrm{h})|\, i = 1, ..., m\}$.

2. Starting from $\boldsymbol{x}(s)$ with the same input $\boldsymbol{u}(t)$, compute the controlled nature run. We obtain $\boldsymbol{x}(s + 6\,\mathrm{h})$ and the 6-h maximum defined by $\max_{1\le j\le N,\, s\le t<s+6\,\mathrm{h}} X_j(t)$.

3. Generate noisy observations $y_j(s + 6\,\mathrm{h}) = X_j(s + 6\,\mathrm{h}) + \varepsilon_j$, where ε_j denotes independent white Gaussian noise with zero mean and unit standard deviation.

4. Assimilate the data using the LETKF described in Section 2.2, obtaining the analysis ensemble $\{\boldsymbol{x}^{a(i)}(s + 6\,\mathrm{h})|\, i = 1, ..., m\}$ at $s + 6$ h.

5. Perform a T-d ensemble forecast under the intervention-off scenario (Section 2.3). Starting from $\{\boldsymbol{x}^{a(i)}(s)|\, i = 1, ..., m\}$ with the input in Eq. (2), integrate Eq. (1) to yield a T-d forecast $\tilde{\boldsymbol{X}}(t)$ over $s \le t < s + 7$ d.

6. If ALERT flag is OFF and one of the ensemble members in the T-d forecast exceeds the upper threshold 14.217 (that is, $\max_{1\le j\le N,\, s\le t<s+T\,\mathrm{d}} \tilde{X}_j(t) > 14.217$), set ALERT=ON and ELAPSE=0 and go to step 9. Otherwise, proceed to step 7.

https://doi.org/10.5194/egusphere-2025-987
Preprint. Discussion started: 21 March 2025

7. Else if ALERT flag is ON and all ensemble members in the T-d forecast remain below the lower threshold 13.5 (that is, $\max_{1\le j\le N,\, s\le t<s+7\,\mathrm{d}} \tilde{X}_j(t) < 13.5$), set ALERT=OFF, choose the intervention-off scenario from the next 6-h cycles ($t > s + 6$ h), and return to step 1, advancing the time s by 6 h. Otherwise, go to step 8.

8. Else if ALERT=ON, increment the elapsed time counter (ELAPSE) by 1 and go to step 9.

9. If ALERT=ON and ELAPSE is zero or a multiple of 4 (that is, every 24 h), perform T-d ensemble forecasts of all intervention scenarios in Eq. (3). For each scenario, obtain the maximum, $M(s) = \max_{1\le j\le N,\, s\le t<s+T\ \mathrm{d},\, i=1,..,m} \tilde{X}_j^{(i)}(t)$. Choose the best scenario on $\boldsymbol{u}(t)$ that minimizes $M(s)$, including also the intervention-off scenario, and return to step 1, advancing the time s by 6 h.

The algorithm starts from $s = 0$ with ALAERT=OFF, ELAPSE=0, and $\boldsymbol{u}(0) = \mathbf{0}$.

Author contributions. T.M. conceived the study and conducted the analyses with contributions from K.T., S.K., N.F., and A.O. All authors discussed and interpreted the results. The manuscript was written by all authors, with T.M. preparing the first draft.

Competing interests. The authors declare that they have no competing financial interests.

Acknowledgements. T.M. thanks Daiya Shiojiri for his support on LETKF implementation. This study was partly supported by the JST Moonshot R&D (JPMJMS2389).

https://doi.org/10.5194/egusphere-2025-987
Preprint. Discussion started: 21 March 2025

References

Cini, M., Zappa, G., Ragone, F., and Corti, S.: Simulating AMOC tipping driven by internal climate variability with a rare event algorithm, npj Clim. Atmos. Sci., 7, 31, https://doi.org/10.1038/s41612-024-00568-7, 2024.

Del Moral, P. and Garnier, J.: Genealogical particle analysis of rare events, Ann. Appl. Probab., 15, 2496–2534, https://doi.org/10.1214/105051605000000566, 2005.

Henderson, J. M., Hoffman, R. N., Leidner, S. M., Nehrkorn, T., and Grassotti, C.: A 4D-Var study on the potential of weather control and exigent weather forecasting, Q. J. R. Meteorol. Soc., 131, 3037–3051, https://doi.org/10.1256/qj.05.72, 2005.

Hunt, B. R., Kostelich, E. J., and Szunyogh, I.: Efficient data assimilation for spatiotemporal chaos: A local ensemble transform Kalman filter, Phys. D: Nonlinear Phenom., 230, 112–126, https://doi.org/10.1016/j.physd.2006.11.008, 2007.

IPCC: Framing, Context, and Methods. In Climate Change 2021 – The Physical Science Basis: Working Group I Contribution to the Sixth Assessment Report of the Intergovernmental Panel on Climate Change, chap. 1, p. 147–286, Cambridge University Press, https://doi.org/10.1017/9781009157896.003, 2023.

Kawasaki, F. and Kotsuki, S.: Leading the Lorenz-63 system toward the prescribed regime by model predictive control coupled with data assimilation, Nonlinear Process. Geophys., 31, 319–333, https://doi.org/10.5194/npg-31-319-2024, 2024.

Kotsuki, S. and Bishop, C. H.: Implementing hybrid background error covariance into the LETKF with attenuation-based localization: experiments with a simplified AGCM, Mon. Weather Rev., 150, 283–302, https://doi.org/10.1175/MWR-D-21-0174.1, 2022.

Kotsuki, S., Shiraishi, K., and Okazaki, A.: Ensemble data assimilation to diagnose AI-based weather prediction model: a case with ClimaX version 0.3. 1, arXiv [preprint], arXiv:2407.17781, 2024.

Lorenz, E. N.: Predictability: A problem partly solved, in: Proc. Seminar on Predictability, vol. 1, Reading, 1996.

Lorenz, E. N. and Emanuel, K. A.: Optimal sites for supplementary weather observations: simulation with a small model, J, Atmos. Sci., 55, 399–414,

Miyoshi, T. and Sun, Q.: Control Simulation Experiment with the Lorenz's Butterfly Attractor, Nonlinear Processes in Geophysics, 29, 133–139, 2022.

Nagai, R., Bai, Y., Ogura, M., Kotsuki, S., and Wakamiya, N.: Evaluation of effectiveness of intervention strategy in control simulation experiment through comparison with model predictive control, Nonlinear Process. Geophys., 2024, 1–16, https://doi.org/10.5194/npg-2024-26, 2024.

Ohtsuka, T., Okazaki, A., Ogura, M., and Kotsuki, S.: Convex Optimization of Initial Perturbations toward Quantitative Weather Control, arXiv [preprint], arXiv:2405.19546, 2024.

Palmer, T. and Hagedorn, R.: Predictability of weather and climate, Cambridge University Press, 2006.

Price, I., Sanchez-Gonzalez, A., Alet, F., Andersson, T. R., El-Kadi, A., Masters, D., Ewalds, T., Stott, J., Mohamed, S., Battaglia, P., et al.: Probabilistic weather forecasting with machine learning, Nature, 637, 84–90, https://doi.org/10.1038/s41586-024-08252-9, 2025.

Ragone, F., Wouters, J., and Bouchet, F.: Computation of extreme heat waves in climate models using a large deviation algorithm, in: Proc. Natl. Acad. Sci., 115, 24–29, https://doi.org/10.1073/pnas.1712645115, 2018.

Sauer, J., Demaeyer, J., Zappa, G., Massonnet, F., and Ragone, F.: Extremes of summer Arctic sea ice reduction investigated with a rare event algorithm, Climate Dynamics, 62, 5219–5237, https://doi.org/https://doi.org/10.1007/s00382-024-07160-y, 2024.

Sawada, Y.: Ensemble Kalman filter meets model predictive control in chaotic systems, SOLA, 20, 400–407, https://doi.org/10.48550/arXiv.2403.06371, 2024a.

https://doi.org/10.5194/egusphere-2025-987
Preprint. Discussion started: 21 March 2025

Sawada, Y.: Quest for an efficient mathematical and computational method to explore optimal extreme weather modification, arXiv [preprint], arXiv:2405.08387, 2024b.

Sun, Q., Miyoshi, T., and Richard, S.: Control simulation experiments of extreme events with the Lorenz-96 model, Nonlinear Process. Geophys., 30, 117–128, https://doi.org/10.5194/npg-30-117-2023, 2023.

Willoughby, H., Jorgensen, D., Black, R., and Rosenthal, S.: Project STORMFURY: a scientific chronicle 1962–1983, Bull. Am. Meteorol. Soc., 66, 505–514,

Wouters, J., Schiemann, R. K., and Shaffrey, L. C.: Rare event simulation of extreme European winter rainfall in an intermediate complexity climate model, J. Adv. Model. Earth Sy., 15, e2022MS003 537, https://doi.org/10.1029/2022MS003537, 2023.